0026-895X/01/6003-497–506$3.00
MOLECULAR PHARMACOLOGY
Vol. 60, No. 3
973/928556
Mol Pharmacol 60:497–506, 2001
Printed in U.S.A.

Interaction of Barbiturate Analogs with the *Torpedo californica* Nicotinic Acetylcholine Receptor Ion Channel

HUGO R. ARIAS, ELIZABETH A. MCCARDY, MARTIN J. GALLAGHER, and MICHAEL P. BLANTON

Departments of Pharmacology and Anesthesiology, School of Medicine, Texas Tech University Health Sciences Center, Lubbock, Texas (H.R.A., E.A.M., M.P.B.); and Department of Neurology, Washington University School of Medicine, St. Louis, Missouri (M.J.G.)

Received March 21, 2001; accepted June 8, 2001

This paper is available online at http://molpharm.aspetjournals.org

ABSTRACT

Barbiturate-induced anesthesia is a complex mechanism that probably involves several ligand-gated ion channel superfamilies. One of these superfamilies includes the archetypical nicotinic acetylcholine receptor (nAChR), in which barbiturates act as noncompetitive antagonists. In this regard, we used the *Torpedo californica* nAChR and a series of barbiturate analogs to characterize the barbiturate binding site(s) on this superfamily member. [^{14}C]Amobarbital binds to one high-affinity (K_d = 3.7 μM) and several (~11) low-affinity (K_d = 930 μM) sites on the resting and desensitized nAChRs, respectively. Characteristics of the barbiturate binding site on the resting nAChR include: (1) a tight structure-activity relationship. For example, the barbiturate isobarbital [5-ethyl-5′-(2-methylbutyl) barbituric acid] is >10-fold less potent than its formula isomer amobarbital [5-ethyl-5′-(3-methylbutyl) barbituric acid] in inhibiting [^{14}C]amobarbital binding. (2) A binding locus within the pore of the nAChR ion channel. Each of the barbiturate analogs inhibited the binding of [^{3}H]tetracaine or photoincorporation of 3-trifluoromethyl-3-(*m*-[^{125}I]iodophenyl) diazirine in a mutually exclusive manner. (3) Stereoselective binding. The *R*(+)-enantiomers of isobarbital and pentobarbital are ~2-fold more potent in inhibiting 3-trifluoromethyl-3-(*m*-[^{125}I]iodophenyl) diazirine photoincorporation than the *S*(−)-enantiomers. Finally, molecular modeling suggests that within the channel, the pyrimidine ring of the barbiturate is located just above the highly conserved leucine ring (M2–9; e.g., δLeu-265), whereas the 5′ side chain projects downward, and depending upon its conformation, introduces steric hindrance to binding because of the restriction in the lumen of the channel introduced by the leucine side chains.

Barbiturates, as a class of compounds, exert a broad range of pharmacological actions, including sedation, general anesthesia, and anticonvulsant and anxiolytic effects. Many of these actions are exerted by inhibiting or enhancing the action of several ligand-gated ion channel (LGIC) receptors (reviewed in Franks and Lieb, 1994; Krasowski and Harrison, 1999). One of the LGIC superfamilies that may play a role in the pharmacological actions of barbiturates includes both muscle- and neuronal-type nicotinic acetylcholine (nAChR) and type 3 5-hydroxytryptamine (5-HT_3R) excitatory receptors, as well as type A ($GABA_A$R) and type C γ-aminobutyric acid and glycine inhibitory receptors (Galzi and Changeux, 1994; Arias, 2000). For example, there have been recent reports of anesthetic supersensitivity for neuronal nAChRs (Evers and Steinbach, 1997), although the role of neuronal nAChRs in barbiturate-induced anesthesia is considered questionable (Downie et al., 2000). Although a wealth of pharmacological data has accumulated with respect to the interaction of barbiturates with the $GABA_A$R, a barbiturate binding site(s) has yet to be identified (Serafini et al., 2000). Based on the attractive hypothesis by Eger et al. (1997), who states that general anesthetics may produce immobility and amnesia by interacting with two different target sites, barbiturate molecules might bind different ion channel receptors (e.g., $GABA_A$R and neuronal nAChRs), where each specific interaction would result in a particular pharmacological action.

The low density of $GABA_A$Rs in neural tissue as well as the complexity of interactions in dealing with an allosteric protein, has made it difficult to directly identify a barbiturate binding site on the $GABA_A$R protein. Fortunately, the *Torpedo californica* muscle-type nAChR provides a model system for examining the interaction of barbiturates with this LGIC superfamily. From *Torpedo* electroplaque tissue,

This research was supported in part by National Institutes of Health Grant R29-NS35786 (M.P.B.).

ABBREVIATIONS: LGIC, ligand-gated ion channel; nAChR, nicotinic acetylcholine receptor; 5-HT_3R, type 3 5-hydroxytryptamine receptor; $GABA_A$R, type A γ-aminobutyric acid receptor; NCA, noncompetitive antagonist; [^{125}I]TID, 3-trifluoromethyl-3-(*m*-[^{125}I]iodophenyl) diazirine; [^{3}H]TCP, [piperidyl-3,4-^{3}H (N)]-(*N*-(1-(2-thienyl)cyclohexyl)-3,4-piperidine; PCP, phencyclidine; CCh, carbamylcholine; dansyltrimethylamine, [1-(dimethylamino)-napthalene-5-sulfonamido]ethyltrimethylammonium perchlorate; HPLC, high-performance liquid chromatography; amobarbital, 5-ethyl-5′-(3-methylbutyl) barbituric acid; amylbarbital, 5-ethyl-5′-amyl barbituric acid; isobarbital, 5-ethyl-5′-(2-methylbutyl) barbituric acid; pentobarbital, 5-ethyl-5′-(1-methylbutyl) barbituric acid; VDB, vesicle dialysis buffer.

postsynaptic membranes that contain nAChRs at high specific activity (~50% of total membrane protein) can be easily obtained and therefore the receptor is amenable to many different methodological approaches, including direct radioligand binding studies. Furthermore, the nAChR and $GABA_AR$ not only exhibit amino acid sequence homology but also, and perhaps more importantly, it is becoming increasingly evident that these two receptors (and each of the LGIC members) share considerable structural homology (Galzi and Changeux, 1994). Barbiturates act as noncompetitive antagonists (NCA) of nAChR function and previous studies have demonstrated the presence of a stereoselective, functional binding site on the receptor (reviewed in Tonner and Miller, 1995; Dilger et al., 1997). The nAChR exists in at least three interconvertible conformations: a resting (closed) state; an open channel state; and a nonconducting desensitized state (Corringer et al., 1999). It is evident that barbiturate interaction is highly dependent on the conformational state of the receptor (de Armendi et al., 1993).

In this study, we wished to more fully characterize the interaction of barbiturates with the resting and desensitized states of the nAChR by identifying important structure-activity relationships for barbiturate binding in each receptor conformation and by identifying a specific binding site(s). First, we examined the equilibrium binding of [^{14}C]amobarbital to the *Torpedo* nAChR in each conformation and then tested the ability of different barbiturates and formula isomers of a given barbiturate to displace [^{14}C]amobarbital binding to the receptor. Next, we identified the barbiturate-binding site on the resting and desensitized nAChR by characterizing barbiturate interaction with well-characterized NCAs. For the resting state of the nAChR, the NCAs [^{3}H]tetracaine and 3-trifluoromethyl-3-(*m*-[^{125}I]iodophenyl) diazirine ([^{125}I]TID) were used. These ligands bind to a single high-affinity site on the resting nAChR. Based on the binding and photoincorporation properties, a binding site in the pore of the ion channel in the resting state has been determined for each NCA (White et al., 1991; White and Cohen, 1992; Gallagher and Cohen, 1999; Middleton et al., 1999). For the desensitized state, the NCAs [piperidyl-3,4-^{3}H (N)]-(*N*-(1-(2-thienyl)cyclohexyl)-3,4-piperidine ([^{3}H]TCP) and quinacrine were used. TCP is the structural analog of phencyclidine (PCP), which binds to a single high-affinity site in the desensitized channel believed to be located near the serine ring (position 6) of the M2 transmembrane domain (reviewed in Arias, 1998). Newer data indicate that PCP effectively binds to residues in the open channel at position 6, 8, and 10 (e.g., M2–6, M2–8, and M2–10) (Eaton et al., 2000). The fluorescent NCA quinacrine also binds to a single high-affinity site on the desensitized nAChR, but at a nonluminal binding site believed to be located at the nonannular lipid domain of the receptor (Arias, 1997; reviewed in Arias, 1998). Finally, the stereoselectivity of barbiturate binding was examined and a molecular model of the binding site in the resting nAChR channel constructed.

Experimental Procedures

Materials. [^{3}H]TCP (57.6 Ci/mmol) was obtained from New England Nuclear Research Products (Boston, MA), [^{125}I]TID (~10 Ci/mmol) from Amersham Pharmacia Biotech (Piscataway, NJ) and both were stored in ethanol at −20°C and 4°C, respectively. [^{3}H]Tetracaine (36 Ci/mmol) was a gift from Dr. Jonathan Cohen (Harvard Medical School, Boston, MA), [^{14}C]amobarbital (50 Ci/mmol) was synthesized by American Radiolabeled Chemicals (St. Louis, MO) and both were stored in ethanol at −20°C. Amylbarbital [5-ethyl-5′-amyl barbituric acid] and isobarbital [5-ethyl-5′-(2-methylbutyl) barbituric acid] were synthesized by Gateway Chemical Technology (St. Louis, MO). Quinacrine dihydrochloride, suberyldicholine dichloride, carbamylcholine chloride (CCh), proadifen, amobarbital hydrochloride, pentobarbital hydrochloride, tetracaine, and PCP were purchased from Sigma Chemical Co. (St. Louis, MO). [1-(Dimethylamino) napthalene-5-sulfonamido] ethyltrimethylammonium perchlorate (dansyltrimethylamine) was obtained from Pierce Chemical Co. (Rockford, IL). Other organic chemicals were of the highest purity available.

Preparation of nAChR-Rich Membranes. nAChR-rich membranes were prepared from frozen *T. californica* electric organs obtained from Aquatic Research Consultants (San Pedro, CA) by differential and sucrose density gradient centrifugation, as described previously (Pedersen et al., 1986). The specific activities of these membrane preparations were determined by the decrease in dansyltrimethylamine (6.6 μM) fluorescence produced by the titration of suberyldicholine into receptor suspensions (0.3 mg/ml) in the presence of 100 μM PCP and ranged between 1.1 and 1.2 nmol of suberyldicholine binding sites/mg of total protein (0.55–0.60 nmol nAChR/mg protein). Dansyltrimethylamine excitation and emission wavelengths were 280 and 546 nm, respectively. To reduce stray-light effects a 530-nm cutoff filter was placed in the path of the dansyltrimethylamine emission beam. The nAChR membrane preparations (in ~36% sucrose, 0.02% NaN_3) were stored at −80°C.

Purification of Barbiturate Enantiomers. The *R*(+)- and *S*(−)- enantiomers of pentobarbital and isobarbital were purified by chiral HPLC using a Nucleodex permethylated β-cyclodextrin column (200 × 4 mm; Machery-Nagel, Easton, PA). The solvent methanol/water/triethylammonium acetate, pH 4.0 (adjusted with acetic acid), was used as the mobile phase in the proportion 65:35:0.1 or 45:55:0.1 (v/v/v) for separation of pentobarbital or isobarbital enantiomers, respectively (Tomlin et al., 1999). An isocratic elution gradient was employed (0.2 ml/min) and the elution of each enantiomer was monitored by absorbance at 240 nm. The final concentration and purity (>90%) of each enantiomer was determined using HPLC peak heights and a standard concentration curve.

Equilibrium Binding of [^{14}C]Amobarbital to nAChR Membranes. The binding of [^{14}C]amobarbital to native nAChR-rich membranes was determined by a centrifugation assay similar to that described for [^{3}H]dizocilpine binding (Arias et al., 2001). Briefly, nAChR membranes (0.3 μM nAChR) were suspended in vesicle dialysis buffer (VDB, 10 mM MOPS, 100 mM NaCl, 0.1 mM EDTA, and 0.02% NaN_3, pH 7.5) with increasing concentrations of [^{14}C]amobarbital in the absence (resting state) or in the presence of 1 mM CCh (desensitized state), at a final volume of 150 μl. [^{14}C]Amobarbital/amobarbital concentration ratios of approximately 0.53 and 0.027 were used in the experiments with nAChRs in the resting and in the desensitized states, respectively; thus, the actual amobarbital concentration was the sum of [^{14}C]amobarbital + unlabeled amobarbital. The final concentration of amobarbital ranged between 0.3 and 13 μM and between 20 and 800 μM, for experiments with nAChRs in the resting or desensitized state, respectively. To determine nonspecific [^{14}C]amobarbital binding, a parallel set of tubes was prepared containing 60 μM tetracaine (resting state experiments) or 100 μM PCP (desensitized state experiments). We used these drug concentrations to obtain nonspecific binding because tetracaine binds with high affinity [dissociation constant (K_d) = 0.5 μM; Middleton et al., 1999] to the nAChR in the resting state and PCP binds with high affinity (K_d = 0.46 μM; Arias, 1999) to the desensitized nAChR. The membrane suspensions were equilibrated for 1 h at room temperature. Bound ([B]) amobarbital was then separated from the free ([F]) ligand by centrifugation at 18,000 rpm for 1 h using a JA-20 rotor in a Beckman J2-HS centrifuge (Beckman Coulter, Inc., Fullerton, CA).

After centrifugation, 50-μl aliquots of the supernatant were removed and assayed for total radioactivity in 3 ml of Bio-Safe II (Research Products International Corp., Mount Prospect, IL) using a Packard 1900 TR scintillation counter (Packard, Meriden, CT). The remainder of the supernatant was aspirated, the tubes inverted, allowed to drain for 30 min, and then any residual liquid was removed with a cotton swab. The pellets were resuspended in 100 μl of 10% SDS, transferred to scintillation vials with 3 ml of Bio-Safe II, and the radioactivity (^{14}C dpm) was determined.

Using the graphics program Prism (GraphPad Software, San Diego, CA), binding data were fit to the Rosenthal-Scatchard plot (Scatchard, 1949) using the equation:

$$[B]/[F] = -([B]/K_d) + (B_{max}/K_d) \quad (1)$$

where B_{max}, the number of amobarbital binding sites, can be estimated from the x-intersect (when y = 0) of the plot [B]/[F] versus [B]. The number of amobarbital binding sites per receptor is then calculated from the concentration of nAChRs (0.3 μM) and the values are reported in Table 1. The K_d value of amobarbital is obtained from the negative reciprocal of the slope (Table 1).

Barbiturate-Induced Inhibition of [^{3}H]Tetracaine, [^{14}C]Amobarbital, and [^{3}H]TCP Binding and [^{125}I]TID Photoincorporation. To determine the effect of barbiturates on the specific binding of [^{3}H]tetracaine, [^{14}C]amobarbital, [^{3}H]TCP, or on [^{125}I]TID photoincorporation into the nAChR, 0.2 μM nAChR native membranes were suspended in 8 ml of VDB buffer with either ~11 nM [^{3}H]tetracaine, 7.5 μM [^{14}C]amobarbital, or ~430 nM [^{125}I]TID in the absence of CCh (resting state), or with ~6.5 nM [^{3}H]TCP in the presence of 0.4 mM CCh (desensitized state). The total volume was then divided into aliquots, and increasing concentrations of a given barbiturate or barbiturate enantiomer were added from ethanolic stock solutions (ethanol concentration <1%) to each tube and the membrane suspension allowed to incubate for 2.5 h at room temperature. For [^{125}I]TID photolabeling experiments, membranes were then irradiated for 7 min at a distance of <1 cm with a 365-nm lamp (Spectroline model EN-280L; Spectronics, Westbury, NY) and labeled polypeptides separated by SDS-polyacrylamide gel (Blanton et al., 2000). For competition binding experiments, after centrifugation (18,000 rpm for 1 h) of the samples, the ^{3}H- or ^{14}C-containing pellets were resuspended in 100 μl of 10% SDS and transferred to a scintillation vial with 5 ml of Bio-Safe II. The bound fraction was determined by scintillation counting, with nonspecific binding determined in the presence of 200 μM amobarbital (resting state experiments) or 200 μM proadifen (desensitized state experiments). For [^{125}I]TID photolabeling experiments, the polyacrylamide gel bands containing the nAChR γ-subunit were excised and the amount of ^{125}I was measured (cpm) with a Packard Cobra II gamma counter. Nonspecific [^{125}I]TID photoincorporation into the γ-subunit was determined in the presence of 0.4 mM CCh as described in Blanton et al. (2000).

The concentration-response data were curve-fit by nonlinear least-squares analysis (one-site competition) using the program Prism and the corresponding IC_{50} values were calculated. Taking into account that the nAChR presents a single high-affinity binding site either for tetracaine (Middleton et al., 1999), TID (White et al., 1991), TCP (Katz et al., 1997, and references therein), or for amobarbital (this article), the observed IC_{50} values were transformed into K_i values using the Cheng-Prusoff relationship (Cheng and Prusoff, 1973):

$$K_i = IC_{50}/\{1 + ([NCA]/K_d^{NCA})\} \quad (2)$$

where [NCA] is the initial concentration of the labeled noncompetitive antagonist ([^{3}H]tetracaine, [^{3}H]TCP, [^{14}C]amobarbital, or [^{125}I]TID) and K_d^{NCA} is the dissociation constant for tetracaine (0.5 μM; Middleton et al., 1999), TCP (~0.2 μM; Katz et al., 1997), TID (4 μM; White et al., 1991), or amobarbital (3.7 μM; see Table 1), respectively.

Effect of Pentobarbital on Quinacrine Binding to the Desensitized nAChR. To determine whether barbiturates interact competitively with the quinacrine binding site on the desensitized nAChR, which is located at the nonannular lipid domain of the nAChR (Arias, 1997; reviewed in Arias, 1998), the effect of pentobarbital on the apparent K_d of quinacrine was measured as described previously (Arias, 1997; Arias et al., 2001). Briefly, direct titrations of quinacrine into nAChR suspensions (0.3 μM) in VDB, CCh (1 mM), in the absence or in the presence of proadifen (200 μM), and different concentrations of pentobarbital to determine the apparent K_d values were assessed in an SLM-Aminco-Bowman Series 2 Luminiscence Spectrometer using 0.5 × 0.5-cm quartz cuvettes. Proadifen was added to define the specific or proadifen-sensitive fluorescence associated with the binding of quinacrine to its high-affinity site on the desensitized nAChR. The nAChR native membrane suspensions containing pentobarbital were allowed to incubate for at least 3 h and up to 5 h at room temperature before the beginning of the titration. A stock solution of 16 mM pentobarbital was prepared in VDB. Quinacrine excitation and emission wavelengths were 450 and 502 nm, respectively. To reduce stray-light effects, a 450-nm narrow band and a 495-nm cutoff filter was placed in the path of excitation and emission beams, respectively.

Estimates of the apparent K_d values of quinacrine were made by fitting the plots of the specific (proadifen-sensitive) changes in quinacrine fluorescence versus added ligand concentration to a four-parameter logistic equation (sigmoid).

To determine the apparent inhibition constant (K_i) of pentobarbital from the quinacrine displacement experiments, a Schild-type plot was used according to the following equation (Schild, 1949):

$$\log[(K_d^{pentobarbital}/K_d) - 1] = \log(pA_2) - \log K_i \quad (3)$$

where K_d and $K_d^{pentobarbital}$ are the apparent dissociation constants of quinacrine in the absence or presence, respectively, of a certain concentration of pentobarbital and pA_2 is the negative logarithm of the concentration of pentobarbital that reduces the apparent affinity of quinacrine by a factor of 2. In other words, when $K_d^{pentobarbital} = 2K_d$, then $\log[(K_d^{pentobarbital}/K_d) - 1] = 0$, and $\log(pA_2) = \log K_i$. In this regard, the K_i value can be graphically calculated as the antilog of the x-intersect (when y = 0) from the $\log[(K_d^{pentobarbital}/K_d) - 1]$ versus log[pentobarbital] plot. To determine whether the observed displacement was elicited by a steric or an allosteric mechanism, the slope of the Schild plot was considered.

Results

Equilibrium Binding of [^{14}C]Amobarbital to nAChR-Rich Membranes. Initial studies were done to confirm the results of Dodson et al. (1987) that demonstrated the presence of saturable high-affinity binding site for amobarbital on the resting *T. californica* nAChR. Secondly, we wished to characterize the binding of amobarbital to the desensitized nAChR.

Resting State. In the absence of agonist (i.e., the resting state), [^{14}C]amobarbital binding to nAChR membranes (7.5 μM [^{14}C]amobarbital, 0.3 μM nAChR) was reduced 38% by the addition of an excess (125 μM) of unlabeled amobarbital (446 versus 273 pmol/mg protein). Addition of an excess of the NCA tetracaine (60 μM) reduced the binding of [^{14}C]amobarbital to the receptor to a level equivalent to that observed with an excess of amobarbital, whereas addition of the competitive antagonist α-bungarotoxin (10 μM) had very little effect on the total binding (410 pmol/mg). These results are similar to those reported by Dodson et al. (1987); therefore, we proceeded to more fully characterize the binding of [^{14}C]amobarbital to the resting nAChR, using an excess (60 μM) of tetracaine to define the level of displaceable (specific) binding. Figure 1A shows the total, nonspecific, and specific

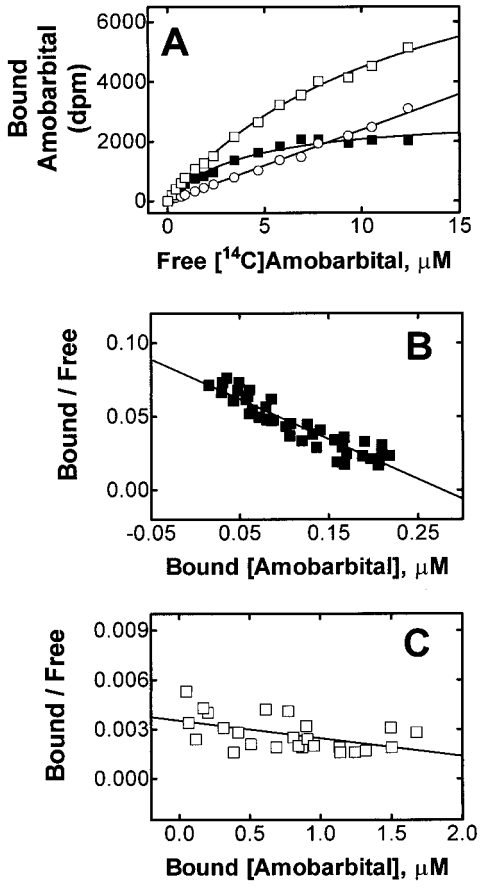

Fig. 1. [^{14}C]Amobarbital binding to nAChR-rich membranes in the resting and desensitized state. A, total (□), nonspecific (○), and specific (■) [^{14}C]amobarbital binding in the resting state. nAChR-rich membranes (0.3 μM) were equilibrated (1 h) with increasing concentrations of [^{14}C]amobarbital (0.3–13 μM) in the absence of CCh. nAChR membranes were then centrifuged and the amount of ^{14}C cpm contained in the pellets was measured as described under *Experimental Procedures*. Nonspecific binding was determined in the presence of tetracaine (60 μM). Specific or tetracaine-sensitive [^{14}C]amobarbital binding is defined as total minus nonspecific [^{14}C]amobarbital binding. B, Rosenthal-Scatchard plots for [^{14}C]amobarbital specific binding in the resting state. C, Rosenthal-Scatchard plots for [^{14}C]amobarbital specific binding in the desensitized state (i.e., in the presence of 1 mM CCh). In this case, the specific binding is defined as total (determined in the concentration range of 20 to 800 μM [^{14}C]amobarbital, data not shown) minus the nonspecific [^{14}C]amobarbital binding (determined in the presence of 100 μM PCP). The K_d values in the resting and desensitized states were determined from the negative reciprocal of the slope of three separate experiments according to eq. 1, then averaged, and finally summarized in Table 1. These plots are the result of three different experiments with calculated values reported ± S.D.

[^{14}C]amobarbital binding to nAChR native membranes. Figure 1B shows the Rosenthal-Scatchard plot for this specific binding. These experimental results indicate the existence of a single (0.89 ± 0.14 binding sites/nAChR) high-affinity (K_d = 3.7 ± 0.7 μM) amobarbital binding site on the *T. californica* muscle-type nAChR when it is in the resting state (Table 1).

Desensitized State. To assess [^{14}C]amobarbital binding to the desensitized nAChR (in the presence of 1 mM CCh), higher concentrations of [^{14}C]amobarbital were used and the addition of 100 μM unlabeled PCP was used to determine nonspecific binding (Fig. 1C). The K_d and the stoichiometry were difficult to calculate accurately because of the low level of specific binding. However, we estimate that the nAChR in the desensitized state bears approximately 11 low-affinity (K_d = 940 ± 380 μM) amobarbital binding sites (Table 1).

TABLE 1

Dissociation constant (K_d) and stoichiometry of amobarbital binding to nAChRs in the desensitized and resting state.

The K_d values in the nAChR resting state were obtained from the negative reciprocal of the slope of Fig. 1B, according to eq. 1. The values in the desensitized state were estimated from Fig. 1C. The number of amobarbital binding sites per nAChR in the resting state was obtained from the *x*-intersect of Fig. 1B, according to eq. 1, and considering the concentration of receptor employed (0.3 μM). The stoichiometry in the desensitized state was estimated from Fig. 1C. Values are reported as mean ± S.D. r^2 expresses goodness of the fit.

AChR State	K_d	Stoichiometry Binding Sites/nAChR	r^2
	μM		
Resting	3.7 ± 0.7	0.89 ± 0.14	0.86
Desensitized	930 ± 380	11 ± 5	0.25

Inhibition of [^{14}C]Amobarbital Binding to the Resting nAChR with Barbiturate Analogs. The effect of barbiturates on displaceable [^{14}C]amobarbital binding to the resting nAChR was examined by centrifugation assay. As expected, amobarbital (Fig. 2) displaced [^{14}C]amobarbital binding in a concentration-dependent fashion (Fig. 3) with a K_i value of 4 μM (Table 2), which is nearly identical to the determined K_d (3.7 μM, Table 1). Pentobarbital also displaced [^{14}C]amobarbital binding in a concentration-dependent fashion, but with a K_i value (38 μM) that is 10-fold

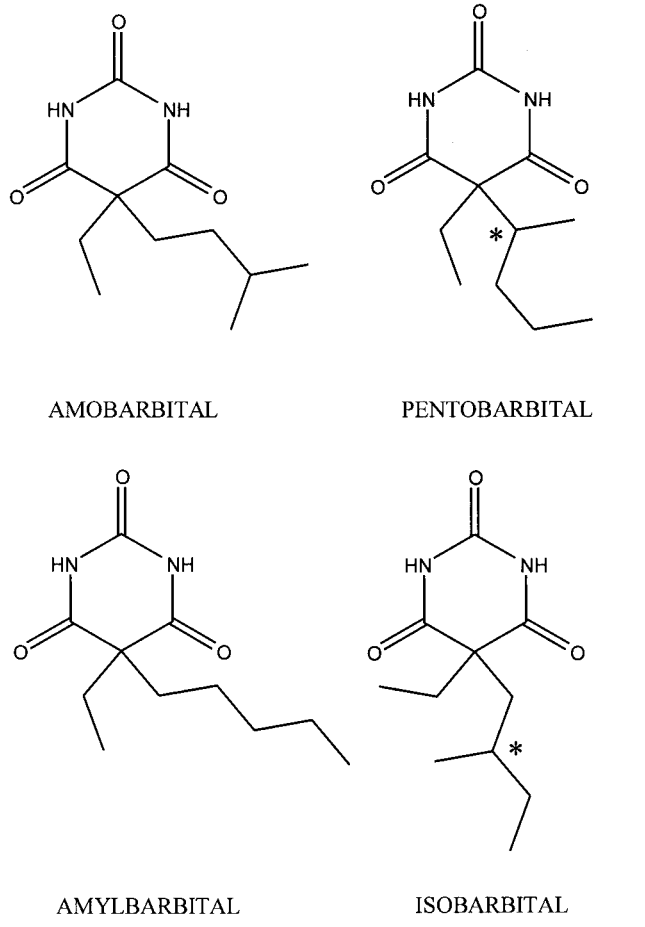

Fig. 2. Chemical structures of barbiturate analogs. The chemical structure of amobarbital, amylbarbital, pentobarbital, and isobarbital are shown. The asterisks (*) indicate the position of the chiral carbon on both pentobarbital and isobarbital.

higher than that of amobarbital. This result is somewhat surprising given that pentobarbital and amobarbital have identical empirical formulas, being formula isomers (Fig. 2) that differ in the point of branching on the 5′ side chain [5′(1-methylbutyl) versus 5′(3-methylbutyl), respectively]. Furthermore, the two barbiturates have nearly identical octanol/water partition coefficients and therefore physicochemical differences such as hydrophobicity are not likely the source of differences in binding affinity. Noting this surprising difference in potency, Dodson et al. (1990) suggested that the simplest explanation was steric hindrance for binding to the barbiturate site on the resting nAChR. To explore this further, we synthesized and tested two additional formula isomers: isobarbital [5′(2-methylbutyl)] and amylbarbital (5′-amyl) (see chemical structures in Fig. 2). Amylbarbital, in which the 5′ side chain has no branching, displaced [^{14}C]amobarbital binding with a potency (K_i = 2.6 μM) that was even slightly greater that that of amobarbital (Fig. 3). In contrast, isobarbital had a potency (K_i = 54 μM) that was slightly less than that of pentobarbital. Remarkably, by moving the point of branching by a single carbon atom (isobarbital to amobarbital) the result is a 10-fold shift in potency (i.e., binding affinity).

Barbiturate-Induced Inhibition of [^{125}I]TID and [^{3}H]Tetracaine Binding to the Resting nAChR. To more fully examine the molecular determinants of the barbiturate-binding site in the resting nAChR, we characterized the interaction of barbiturates with two NCAs (tetracaine and TID). Each of these NCAs has well-characterized binding properties and for each, a binding locus within the resting nAChR channel has been established (White et al., 1991; White and Cohen, 1992; reviewed in Arias, 1998; Gallagher and Cohen, 1999; Middleton et al., 1999). In the absence of agonist, greater than 95% of the [^{125}I]TID photoincorporation into the nAChR γ-subunit reflects labeling of specific residues in the channel-lining M2 segment and can be inhibited by TID (as well as tetracaine) or by addition of agonist (White and Cohen, 1992; Blanton et al., 2000). Each of the barbiturate analogs (e.g., amobarbital, amylbarbital, pentobarbital, and isobarbital) inhibited [^{125}I]TID photoincorporation into the γ-subunit (Fig. 4A) in a concentration-dependent fashion and with potencies and rank order that exactly paralleled inhibition of [^{14}C]amobarbital binding (Table 2). For example, at 120 μM amobarbital, more than 93% of the specific [^{125}I]TID photoincorporation into the γ-subunit is inhibited and the interaction seems to be formally competitive (K_i = 6.9 μM; n_H = 0.96, r^2 = 0.980).

The binding sites for TID and tetracaine in the resting nAChR channel overlap; therefore, it was not surprising that nearly identical results were observed for barbiturate inhibition of [^{3}H]tetracaine binding to the nAChR (Fig. 4B, Table 2). Again, as an example, 120 μM amylbarbital inhibited >97% of the specific [^{3}H]tetracaine binding to the resting nAChR, and the inhibition seems to be formally competitive (K_i = 6.3 μM; n_H = 0.91, r^2 = 0.993). In reciprocal fashion, tetracaine completely displaces specific [^{14}C]amobarbital binding to the resting nAChR (data not shown). This inhibition seems to be formally competitive (n_H = 0.97, r^2 = 0.997); and the K_i value (~0.3 μM) is nearly identical to the reported K_d for tetracaine (0.5 μM; Middleton et al., 1999). For inhibition of [^{14}C]amobarbital, [^{3}H]tetracaine binding, or [^{125}I]TID photoincorporation, the same rank order of potency was observed: amylbarbital > amobarbital ≫ pentobarbital > isobarbital. Finally, with respect to inhibition of [^{125}I]TID photoincorporation into the resting nAChR, additional barbiturates were examined (data not shown) and are listed in order of rank potency: secobarbital (IC_{50} = 123 μM),

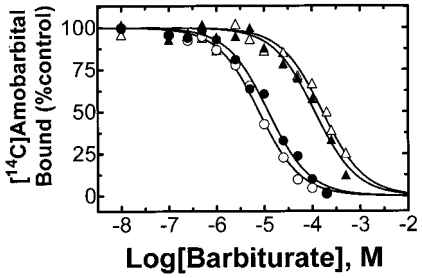

Fig. 3. Barbiturate-induced displacement of [^{14}C]amobarbital binding to nAChRs in the resting state. nAChR-rich membranes (0.2 μM) were equilibrated (1 h) with [^{14}C]amobarbital (7.5 μM), in the presence of increasing concentrations (0.01–200 μM) of amobarbital (●), amylbarbital (○), pentobarbital (▲), and isobarbital (△). The nAChR membranes were then centrifuged and the radioactivity present in the pellets measured as described under *Experimental Procedures*. Nonspecific binding was determined in the presence of 200 μM amobarbital. Each plot is the average of two different experiments. The IC_{50} value for each barbiturate was calculated by nonlinear least-squares fit for a single binding site. K_i values for each barbiturate were calculated using these IC_{50} values according to eq. 2 and summarized in Table 2.

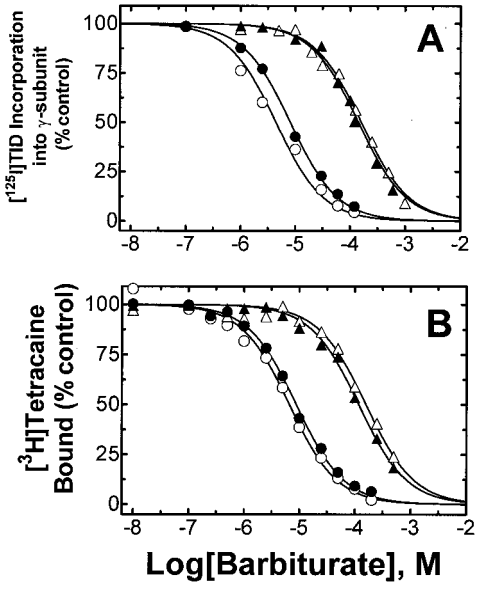

Fig. 4. Barbiturate-induced inhibition of [^{125}I]TID photoincorporation and [^{3}H]tetracaine binding to nAChRs in the resting state. nAChR-rich membranes (0.2 μM) were equilibrated (1 h) with (A) [^{125}I]TID (~430 nM) or (B) [^{3}H]tetracaine (~11 nM), in the presence of increasing concentrations (0.01–200 μM) of either amobarbital (●), amylbarbital (○), pentobarbital (▲), or isobarbital (△). For [^{125}I]TID photolabeling experiments (A), the membrane suspensions were irradiated with 365-nm ultraviolet light for 7 min, the nAChR subunits separated by SDS-polyacrylamide gel electrophoresis, and the ^{125}I cpm in the nAChR γ-subunit measured by gamma counting as described under *Experimental Procedures*. Nonspecific photoincorporation into the γ-subunit was determined in the presence of 400 μM CCh. For [^{3}H]tetracaine competition binding experiments (B), nAChR membranes were centrifuged and the radioactivity present in the pellets was measured as described under *Experimental Procedures*. Nonspecific binding was determined in the presence of 200 μM amobarbital. Each plot is the average of two different experiments. IC_{50} values for each barbiturate were calculated by nonlinear least-squares fit for a single binding site. K_i values for each barbiturate were calculated using these IC_{50} values according to eq. 2 and summarized in Table 2.

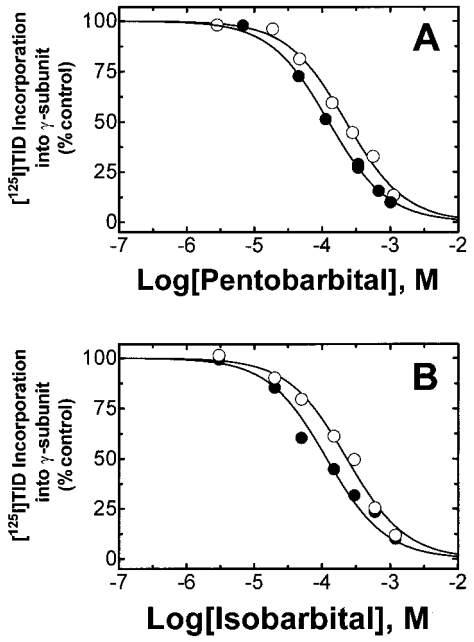

Fig. 5. Barbiturate enantiomer-induced inhibition of [^{125}I]TID photoincorporation into nAChRs in the resting state. nAChR-rich membranes (0.2 μM) were equilibrated (1 h) with [^{125}I]TID (~430 nM), in the presence of increasing concentrations (0.01–200 μM) of barbiturate enantiomers: $R(+)$-pentobarbital (●) and $S(-)$-pentobarbital (○) (A) and $R(+)$-isobarbital (●) and $S(-)$-isobarbital (○) (B). Membrane suspensions were irradiated with 365-nm ultraviolet light for 7 min, the nAChR subunits separated by SDS-polyacrylamide gel electrophoresis, and the ^{125}I cpm in the γ-subunit measured by gamma counting as described under *Experimental Procedures*. Nonspecific photoincorporation into the γ-subunit was determined in the presence of 400 μM CCh. Each plot is the average of two different experiments. IC_{50} values for each barbiturate were calculated by nonlinear least-squares fit for a single binding site. K_i values for each barbiturate were calculated using these IC_{50} values according to eq. 2 and summarized in Table 2.

phenobarbital (366 μM), butabarbital (516 μM), barbital (1800 μM), and hexobarbital (5000 μM). These values are very similar to those reported for inhibition of [^{14}C]amobarbital binding to the resting nAChR (de Armendi et al., 1993).

Stereoselectivity of Barbiturate Inhibition of [^{125}I]TID Photoincorporation into the Resting nAChR. To obtain additional information about the molecular determinants of the barbiturate-binding site in the resting nAChR channel, we next examined the stereoselectivity of barbiturate binding. The $R(+)$- and $S(-)$-enantiomers of pentobarbital and isobarbital were purified by chiral HPLC from a racemic mix of both optical isomers (data not shown). Each enantiomer was then used to displace [^{125}I]TID photoincorporation into the γ-subunit of the resting nAChR (Fig. 5). From these experiments, we found that for both pentobarbital and isobarbital the $R(+)$-enantiomer is about 1.8-fold more potent in inhibiting [^{125}I]TID photoincorporation into the γ-subunit than the $S(-)$-enantiomer (see Table 2). For inhibition of [^{14}C]pentobarbital binding to the resting nAChR, Roth et al. (1989) also found that the $R(+)$-enantiomer of pentobarbital was more potent than the $S(-)$-enantiomer in displacing binding, albeit with slightly greater differences in potency (4-fold; 130 versus 525 μM, respectively).

Barbiturate-Induced Inhibition of [^{3}H]TCP Binding to the Desensitized nAChR. To begin to characterize the low-affinity barbiturate binding site(s) on the desensitized nAChR, we first examined the effect of the same barbiturate analogs on [^{3}H]TCP binding (Fig. 6). TCP, which binds with high affinity to the ion channel in the desensitized state (Katz et al., 1997) is an analog of the dissociative anesthetic and NCA PCP (reviewed in Arias, 1998). Each barbiturate displaced specific [^{3}H]TCP binding to the desensitized nAChR in a concentration-dependent fashion, albeit with substantially reduced potencies relative to those observed for the resting nAChR (Fig. 6A). As an example, 3 mM isobarbital inhibited >80% of the specific [^{3}H]TCP binding to the desensitized receptor and the inhibition seemed to be formally competitive (K_i = 582 μM n_H = 0.94; r^2 = 0.992). For inhibition of [^{3}H]TCP binding to the desensitized nAChR, the barbiturate potencies follow the order: secobarbital (K_i = 136 μM; data not shown) > pentobarbital > isobarbital > amylbarbital ~ amobarbital (see Table 3). This rank order is almost completely opposite that observed in the resting nAChR (see Table 2). Clearly, the binding site determinants in the resting versus desensitized nAChRs are different. Yet, as was the case in the resting state, the $R(+)$-enantiomers of both pentobarbital and isobarbital are approximately 1.7-fold more potent than the $S(-)$-enantiomers in inhibiting [^{3}H]TCP binding to the desensitized nAChR (Fig. 6B). Therefore the binding site in the resting and desensitized state may have some structural features in common.

Given that the [^{14}C]amobarbital equilibrium binding results suggest that there are between 6 and 16 barbiturate binding sites on the desensitized nAChR, we next sought to examine the interaction of barbiturates with quinacrine, an NCA that binds to a site distinct from the channel lumen (Arias, 1997; reviewed in Arias, 1998). The effect of pentobarbital on quinacrine binding was determined. In this regard, the 'apparent' K_d values for quinacrine were determined in the absence and in the presence of increasing concentrations of pentobarbital. Examples of the results of a set of these titrations are shown in Fig. 7A. This figure shows typical quinacrine titrations performed in duplicate as the specific (or proadifen-sensitive) fluorescence of quinacrine when binding to the nAChR in the presence of CCh. The plots were best fit by nonlinear regression for a single binding site. In the presence of pentobarbital, the apparent K_d of quinacrine increased. Thus, to determine the K_i of pentobarbital from the elicited displacement on nAChR-bound quinacrine,

TABLE 2

Inhibition constant (K_i) for select barbiturates and $R(+)$- or $S(-)$-enantiomers determined for inhibition of either binding or photolabeling of NCAs to their respective sites on nAChRs in the resting conformational state

The K_i values (averaged) were calculated using the Cheng-Prusoff relationship (eq. 2) and the IC_{50} values obtained from Figs. 3 ([^{14}C]amobarbital), 4A and 5 ([^{125}I]TID), and 4B ([^{3}H]tetracaine).

Barbiturate	K_i		
	[^{14}C]Amobarbital	[^{3}H]Tetracaine	[^{125}I]TID
		μM	
Amylbarbital	2.6 ± 0.2	6.3 ± 1.0	3.3 ± 0.2
Amobarbital	4.0 ± 0.3	8.5 ± 0.4	6.9 ± 0.4
Pentobarbital			
Racemic	38 ± 4	113 ± 5	129 ± 8
$R(+)$			113 ± 5
$S(-)$			201 ± 12
Isobarbital			
Racemic	54 ± 8	152 ± 12	144 ± 7
$R(+)$			110 ± 24
$S(-)$			209 ± 25

a Schild plot was constructed (Fig. 7B). The K_i value, obtained from the antilog of the x-intersect (when y = 0), was found to be 135 μM. Because the slope from this plot is different from one (0.36 ± 0.20), the calculated K_i should be considered an "apparent K_i". Because a slope value less than unity indicates that the inhibitory process is not mediated by a mutually exclusive action, an allosteric inhibitory mechanism instead is plausible; therefore pentobarbital does not seem to bind to the quinacrine binding locus on the desensitized nAChR. The location of these additional barbiturate binding sites on the desensitized nAChR remains to be established, with sites at the lipid-protein interface being likely candidates.

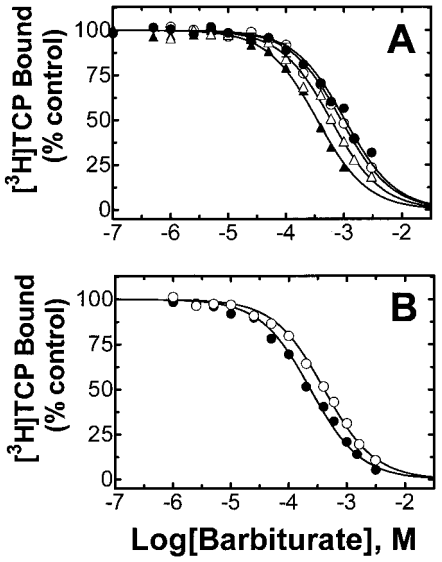

Fig. 6. Barbiturate-induced inhibition of [^{3}H]TCP binding to desensitized nAChRs. nAChR-rich membranes (0.2 μM) were equilibrated (1 h) with [^{3}H]TCP (~6.5 nM), CCh (250 μM), in the presence of increasing concentrations (0.01–200 μM) of the barbiturate amobarbital (●), amylbarbital (○), pentobarbital (▲), or isobarbital (△) (A) and the barbiturate enantiomers $R(+)$-pentobarbital (●) and $S(-)$-pentobarbital (○) (B). The nAChR membranes were centrifuged and the radioactivity present in the pellets was measured as described under *Experimental Procedures*. Nonspecific binding was determined in the presence of 200 μM proadifen. Each plot is the average of two different experiments. IC_{50} values for each barbiturate was calculated by nonlinear least-squares fit for a single binding site. K_i values for each barbiturate were calculated using these IC_{50} values according to eq. 2 and summarized in Table 3.

TABLE 3

Inhibition constant (K_i) for select barbiturates and $R(+)$- or $S(-)$-enantiomers determined by inhibition of [^{3}H]TCP binding to its high-affinity site on the desensitized nAChR

The K_i values (averaged) were calculated using the Cheng-Prusoff relationship (eq. 2) and the IC_{50} values obtained from Fig. 6.

Barbiturate	K_i
	μM
Amobarbital	1017 ± 58
Amylbarbital	872 ± 35
Pentobarbital	
Racemic	338 ± 28
$R(+)$	233 ± 11
$S(-)$	396 ± 15
Isobarbital	
Racemic	
$R(+)$	582 ± 28
$S(-)$	320 ± 43

Discussion

Barbiturate Interaction with the Resting nAChR. The results of equilibrium binding experiments demonstrate that amobarbital binds to a single high-affinity (K_d = 3.7 μM) site on the resting nAChR (Fig. 1). Based on the mutually exclusive nature of barbiturate inhibition of [^{125}I]TID photoincorporation and [^{3}H]tetracaine binding (Fig. 4), this site is localized to the pore of the nAChR ion channel. From studies examining the inhibition of [^{125}I]TID photoincorporation into the receptor by different barbiturates, by formula isomers of amobarbital, and stereoisomers of pentobarbital and isobarbital, it is evident that two basic characteristics dominate barbiturate interaction with the resting channel: (1) a minimal level of barbiturate hydrophobicity and (2) steric hindrance. With respect to barbiturate hydrophobicity, shortening the 5′ chain of amylbarbital or amobarbital (Fig. 2) by three carbons to produce barbital (5-ethyl, 5′-ethyl barbituric acid) reduces the hydrophobic character of the barbiturate molecule and results in a >500-fold reduction in potency for inhibition of [^{125}I]TID photoincorporation or [^{14}C]amobarbital binding (Dodson et al., 1990; de Armendi et al., 1993) to the resting nAChR. On the other hand, extending the length of the chain at the 5-position by an extra carbon (CH_2) converts pentobarbital to secobarbital, resulting in an increase in hydrophobicity as measured by the octanol/water partition

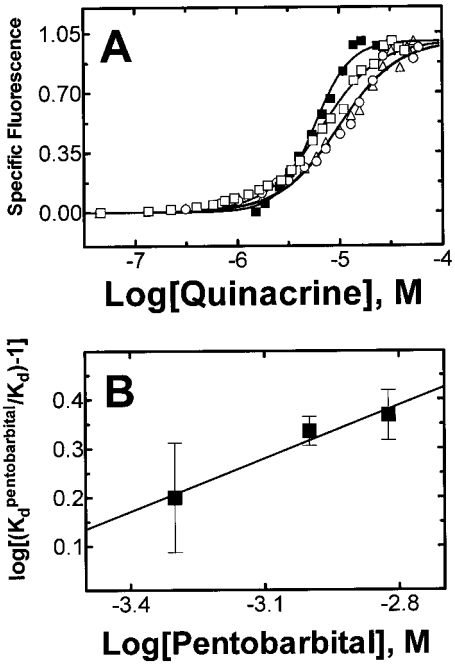

Fig. 7. Pentobarbital-induced inhibition of quinacrine binding to its high-affinity site on the desensitized nAChR. A, specific (proadifen-sensitive) fluorescence of quinacrine in the absence (■) or in the presence of 0.5 (□), 1.0 (○), or 1.5 mM pentobarbital (△). Quinacrine was directly titrated into nAChR-containing membranes (0.3 μM) in the presence of CCh (1 mM), and in the absence (control) or in the presence of pentobarbital. Proadifen (200 μM) was used to determine nonspecific fluorescence. Estimates of the apparent K_d values were made by fitting plots of the specific changes in quinacrine fluorescence versus the added ligand concentration to the equation for a sigmoid curve. These plots are the average of duplicate experiments and are examples of at least four separate determinations. B, Schild plot for the effect of pentobarbital on the apparent K_d value of quinacrine. The pentobarbital apparent K_i value (135 μM) was obtained from the antilog of the x-intersect according to eq. 3. The slope of the plot is 0.36 ± 0.20.

coefficient (Dodson et al., 1990) but with no increase in potency for inhibition of [^{125}I]TID photoincorporation or [^{14}C]amobarbital binding. In other words, high-affinity binding to the nAChR channel site requires that the barbiturate possess a minimum level of hydrophobic character; going beyond that threshold level, however, increased hydrophobicity does not seem to lead to increased binding affinity. The dramatic difference in inhibition potencies between the formula isomers of amobarbital (Figs. 2–4) clearly points out that steric constraints play a significant role in barbiturate binding to the resting nAChR channel. For example, by shifting the branch point on the 5′ chain of amobarbital [5-ethyl, 5′-(3-methylbutyl) barbituric acid] by one carbon closer to the pyrimidine ring [i.e., isobarbital, 5-ethyl, 5′ (2-methylbutyl) barbituric acid] the result is a reduction of >10-fold in the potency of inhibition of [^{14}C]amobarbital (Fig. 3) or [^{3}H]tetracaine binding (Fig. 4B) or [^{125}I]TID photoincorporation (Fig. 4A) into the resting nAChR. The role of steric constraints in barbiturate binding to the resting nAChR channel is further demonstrated by the ~2-fold differences in potency of inhibition between the *R*(+)- and *S*(−)-enantiomers of pentobarbital and isobarbital (Fig. 5).

Competition binding and photolabeling studies argue strongly that in the resting nAChR, the high-affinity barbiturate binding site overlaps that for tetracaine and TID (Figs. 4–5). The binding sites for TID (White and Cohen, 1992; Blanton et al., 2000) and tetracaine (Gallagher and Cohen, 1999) in the resting nAChR channel have been extensively characterized. Tetracaine and TID bind to overlapping sites in the resting channel. For the smaller TID molecule, that site is located between the highly conserved ring of leucine residues (M2–9, e.g., δLeu-265) and the more extracellular ring of valine residues (M2–13, e.g., δVal-269). TID is similar in size to pentobarbital (or amobarbital) and if we model pentobarbital complexed with the resting nAChR channel (see Fig. 8), we see that the barbiturate pyrimidine ring fits nicely in the TID binding site [defined by M2–9 (Fig. 8, yellow) and M2–13 (Fig. 8, red)]. If the barbiturate molecule is oriented such that the 5′ chain extends downward toward the intracellular end of the channel, we see that the restriction in the lumen of the channel introduced by the leucine side chains (M2–9) provides steric hindrance to barbiturate binding depending on the conformation of the 5′ chain (Fig. 8B). We propose that the dramatic difference in inhibition potencies (i.e., binding affinity) between amobarbital (or amylbarbital) and either pentobarbital or isobarbital, result from the ability of the 5′ chain of amobarbital (or amylbarbital) to adopt a more extended conformation compared with pentobarbital (or isobarbital). Therefore, the amobarbital (or amylbarbital) molecule fits better in the narrow crevice [i.e., the channel lumen (~3.5 Å; Unwin, 2000)] created by the ring of the leucine side chains (M2–9). Another possibility is that the side chains of pentobarbital (or isobarbital) have less rotational freedom than amobarbital (or amylbarbital). In either case, the branching on the 5′ chain of pentobarbital (or isobarbital) results in a bulkier conformation that provides steric hindrance to the binding of the barbiturate into the channel lumen.

Barbiturate Interaction with the Desensitized nAChR. From equilibrium binding studies we estimated that amobarbital binds with very low affinity (K_d ~1 mM) to as many as 6 to 16 binding sites on the desensitized nAChR. Despite such a strong preference for interaction with the resting nAChR (~250-fold), we nonetheless wished to characterize the interaction of amobarbital and other barbiturates with the desensitized nAChR. As with the resting

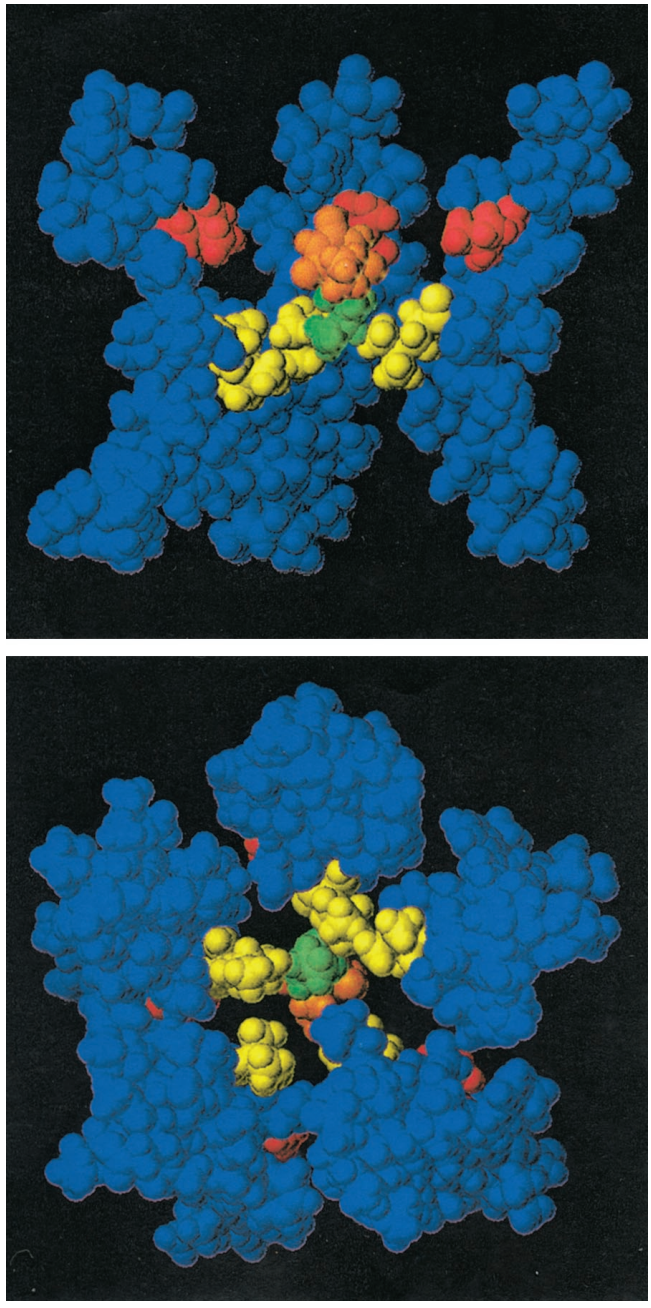

Fig. 8. Model of pentobarbital complexed with the resting nAChR channel. Shown is a molecular dynamics model of the closed (resting state) nAChR ion channel pore (Smith and Sansom, 1998). The structure of pentobarbital was derived by molecular substitution (using Sybyl; Tripos Inc., St. Louis, MO.) of the crystal structure of α-methylamobarbital (Smit and Kanters, 1974). Top, pentobarbital (pyrimidine ring shown in orange) is placed at about the level of residues at position 13 (M2–13, e.g., δVal-269; shown in red). The 1-methylbutyl group of the 5′ chain of pentobarbital (shown in green) provides steric hindrance to pentobarbital binding as a result of the restriction in the channel imposed by the side-chains of residues at position 9 (M2–9, e.g., δLeu-265; shown in yellow). For comparison, the binding site for [^{125}I]TID is defined by residues at M2–9 and M2–13 (White and Cohen, 1992). Two M2 segments are not displayed to better visualize pentobarbital within the pore. Bottom, cross-sectional view of pentobarbital within the channel pore as viewed from the cytoplasmic end.

nAChR, the ability of barbiturates to inhibit binding of the NCA [^{3}H]TCP to the receptor strongly suggests a barbiturate binding site within the desensitized nAChR channel (Fig. 6). For example, amobarbital inhibits [^{3}H]TCP binding to the desensitized nAChR with a K_i value of 1017 μM (Table 3; see also Cohen et al., 1986), a result that is in close agreement with our equilibrium binding results (Table 1). TCP is a close structural analog of PCP whose binding site in the ion channel is believed to be located between the ring of leucine residues (M2–9) and the more cytoplasmic ring of serine residues (M2–6; Eaton et al., 2000). The relative order of barbiturate potencies for inhibition of [^{3}H]TCP binding to the desensitized nAChR are nearly reversed from those for the resting nAChR (compare Tables 2 and 3), suggesting that the structure-activity relationships for binding to the desensitized nAChR are distinct from those for binding to the resting nAChR channel. However, as with the resting nAChR, the *R*(+)-enantiomers of pentobarbital and isobarbital were roughly twice as potent in inhibiting [^{3}H]TCP binding than the *S*(−)-enantiomers, suggesting at least some commonality between the channel binding sites in each conformation. From the equilibrium binding studies, it was estimated that there were as many as 11 binding sites for amobarbital on the desensitized nAChR. Although this value is an approximation, it suggests the presence of additional binding sites on the desensitized nAChR distinct from the ion channel. Barbiturates do not seem to interact with the quinacrine binding site (Fig. 7), which is thought to be located at the nonannular lipid domain (Arias, 1997; reviewed in Arias, 1998), and we are currently conducting additional studies, including photoaffinity labeling experiments with [^{14}C]amobarbital, to identify these additional sites of interaction. One possibility is that at least some of these low-affinity barbiturate-binding sites are located at the lipid-protein interface (annulus) of the desensitized nAChR.

Barbiturate Interaction with the Open Ion Channel. In the nAChR resting state, we found that amobarbital was approximately 20-fold more potent than pentobarbital in inhibiting either [^{14}C]amobarbital or [^{3}H]tetracaine binding, indicating a similar difference in binding affinity to the resting channel. In contrast, the reported inhibition constants for the open channel conformation indicate a much smaller difference (1.4-fold) in potency between these two barbiturates (Yost and Dodson, 1993). Preliminary electrophysiological experiments performed in ALL-11 cells expressing *T. californica* nAChRs suggest that there is 4.9-fold difference in channel-inhibition potency between amobarbital (IC_{50} = 3.2 ± 0.2 μM) and pentobarbital (IC_{50} = 15.6 ± 1.8 μM) (J. Dilger, unpublished observations). Thus, the observed discrepancy may be caused by the differences in the origin of the used nAChR. For instance, the same barbiturates inhibit the mouse muscle nAChR expressed in BC_3-H1 cells with IC_{50} values of 22.8 ± 3.7 (amobarbital) and 22.6 ± 3.0 μM (pentobarbital), respectively (J. Dilger, unpublished observations). The affinity of amobarbital for the open channel of the *T. californica* nAChR is clearly similar to its affinity for the resting state, but both affinities are higher than that for the desensitized nAChR. On the contrary, pentobarbital exhibits a stronger preference for the open channel state than for either the resting or desensitized state (de Armendi et al., 1993; Dilger et al., 1997). There is very little information pertaining to the location of the barbiturate-binding site in the open channel. One study (Yost and Dodson, 1993), in which the triple mutation Ser^{252}Ala (on both α1 subunits) and Thr^{265}Ala (on the β1 subunit) decreased by 3.5-fold the dissociation rate constant of the local anesthetic QX-222 and by 3-fold the IC_{50} value for procaine, but resulted in no affect on amobarbital induced inhibition, suggests that the barbiturate binding site is not located between M2–6 and M2–10 in the open channel (see also Yamakura et al., 2000). Studies aimed at localizing the barbiturate binding site within the nAChR open channel as well as a more detailed characterization of the structure-activity relationship for barbiturate binding, including stereochemistry, are clearly warranted. Once the interaction of barbiturates with each receptor conformation has been fully characterized perhaps then a detailed mechanistic model of barbiturate inhibition of receptor function can be developed.

Table 4
M2 Segment

	◆								□				*							
Mouse AChR α	E	K	M	T	L	S	I	S	V	L	L	S	L	T	V	F	F	L	V	I	V	E
Rat $GABA_AR$ α1	A	R	T	V	F	G	V	T	T	V	L	T	M	T	T	L	S	I	S	A	R	N
RAT GlyR α1	A	R	V	G	L	G	I	T	T	V	L	T	M	T	T	Q	S	S	G	S	R	A
Mouse $5HT_{3A}R$	E	R	V	S	F	K	I	T	L	L	L	G	Y	S	V	F	L	I	I	V	S	D

◆, position 1 of the M2 segment; □, position 9; *, position 13.

Comparison with Other Ligand-Gated Ion Channel Members. As measured by the loss of righting reflex in mice, the *S*(−)-enantiomer of pentobarbital is approximately 2-fold more potent than the *R*(+)-enantiomer for inducing anesthesia and the *S*(−)-enantiomer is approximately twice as potent in potentiating chloride currents that flow through the $GABA_AR$ (Tomlin et al., 1999). Although these results provide evidence that the $GABA_AR$ is the primary target for barbiturate-induced anesthesia, they (i.e., the functional effects and the relative stereoselective potencies) also point out the clear differences in the interaction of barbiturates with the structurally homologous members of this LGIC superfamily (reviewed in Krasowski and Harrison, 1999). On the other hand, barbiturates exhibit similar affinities for the $GABA_AR$ and nAChR, and although the stereoselectivity is reversed, the magnitudes of the differences in stereoisomer potencies are also very similar (Tonner and Miller, 1995; Krasowski and Harrison, 1999). Perhaps there are common binding sites or at least common structural features for barbiturate binding to different members of this LGIC superfamily. For example, in this report, we demonstrate that amobarbital and other barbiturates bind to a single high-affinity site localized within the nAChR channel in the resting conformation. The pore-facing amino acid residues in this region of the channel (i.e., M2–9 through M2–13) are well conserved in each of the different LGIC members, suggesting that a common barbiturate-binding site might exist in each receptor, at least in the resting state (Table 4).

It is striking that identical residues are present in the subunit A of the mouse 5-HT_3R and in the mouse or *T. californica* α1-, β1-, and δ-subunits at positions M2–9 and M2–13. Interestingly, pentobarbital inhibits 5-HT_3R function (Barann et al., 1997). However, it is difficult to reconcile a barbiturate-binding site in the lumen of the $GABA_AR$ (or glycine receptor) with potentiation of agonist-induced currents. To try and resolve these questions, we are presently

pursuing studies aimed at directly measuring [^{14}C]amobarbital binding to affinity-purified 5-HT_{3A}R and $GABA_A$R.

Acknowledgments

We thank Drs. Tina Machu (Texas Tech University Health Sciences Center, Lubbock, TX) and James Dilger (State University of New York at Stony Brook, Stony Brook, NY) for their helpful comments and suggestions. We thank Drs. Nick Franks and Robert Dickinson (Imperial College of Science, Technology and Medicine, London) for providing us with samples of purified *R*(+)- and *S*(−)-pentobarbital to get started and for technical advice. We also thank Dr. Jay Ponder (Washington University School of Medicine, St. Louis, MO) for use of his computer workstation, molecular graphics software, and invaluable assistance. Finally, we thank Drs. Mark Sansom and Graham Smith (University of Oxford, Oxford, England) for kindly providing the coordinates for their kinked α7 M2 molecular model.

References

Arias HR (1997) The high-affinity quinacrine binding site is located at a non-annular lipid domain of the nicotinic acetylcholine receptor. *Biochim Biophys Acta* **1347:** 9–22.

Arias HR (1998) Binding sites for exogenous and endogenous non-competitive inhibitors of the nicotinic acetylcholine receptor. *Biochim Biophys Acta* **1376:**173–220.

Arias HR (1999) 5-Doxylstearate-induced displacement of phencyclidine from its low-affinity binding sites on the nicotinic acetylcholine receptor. *Arch Biochem Biophys* **371:**89–97.

Arias HR (2000) Localization of agonist and competitive antagonist binding sites on nicotinic acetylcholine receptors. *Neurochem Int* **36:**595–645.

Arias HR, McCardy EA and Blanton MP (2001) Characterization of the dizocilpine binding site on the nicotinic acetylcholine receptor. *Mol Pharmacol* **56:**1051–1060.

Barann M, Gother M, Bonisch H, Dybek A and Urban BW (1997) 5-HT_3 receptors in outside-out patches of N1E-115 neuroblastoma cells: basic properties and effects of pentobarbital. *Neuropharmacology* **36:**655–664.

Blanton MP, McCardy EA and Gallagher MJ (2000) Examining the noncompetitive antagonist-binding site in the ion channel of the nicotinic acetylcholine receptor in the resting state. *J Biol Chem* **275:**3469–3478.

Cheng YC and Prusoff WH (1973) Relationships between the inhibition constant (K_i) and the concentration of inhibitor which causes 50 per cent inhibition (IC_{50}) of an enzymatic reaction. *Biochem Pharmacol* **22:**3099–3108.

Cohen JB, Correll LA, Dreyer EB, Kusik IR, Medynski DC and Strnad NP (1986) Interactions of local anesthetics with *Torpedo* nicotinic acetylcholine receptors, in *Molecular and Cellular Mechanisms of Anesthetics* (Roth SH and Miller KW eds.). Plenum Medical Book Company, New York, pp. 111–124.

Corringer J-P, Le Novere N and Changeux J-P (1999) Nicotinic receptors at the amino acid level. *Annu Rev Pharmacol Toxicol* **40:**431–458.

de Armendi AJ, Tonner PH, Bugge B and Miller KW (1993) Barbiturate action is dependent on the conformational state of the acetylcholine receptor. *Anesthesiology* **79:**1033–1041.

Dodson BA, Braswell LM and Miller KW (1987) Barbiturates bind to an allosteric regulatory site on nicotinic acetylcholine receptor-rich membranes. *Mol Pharmacol* **32:**119–126.

Dodson BA, Urh RR and Miller KW (1990) Relative potencies for barbiturate binding to the *Torpedo* acetylcholine receptor. *Br J Pharmacol* **101:**710–714.

Dilger JP, Boguslavsky R, Barann M, Katz T and Vidal AM (1997) Mechanisms of barbiturate inhibition of acetylcholine receptor channels. *J Gen Physiol* **109:**401–414.

Downie DL, Franks NP and Lieb WR (2000) Effects of thiopental and its optical isomers on nicotinic acetylcholine receptors. *Anesthesiology* **93:**774–783.

Eaton MJ, Labarca CG and Eterovic VA (2000) M2 mutations of the nicotinic acetylcholine receptor increase the potency of the non-competitive inhibitor phencyclidine. *J Neurosci Res* **61:**44–51.

Eger EI, Koblin DD, Harris RA, Kendig JJ, Pohorille A, Halsey MJ and Trudell R (1997) Hypothesis: inhaled anesthetics produce immobility and amnesia by different mechanisms at different sites. *Anesth Analg* **84:**915–918.

Evers AS and Steinbach JH (1997) Supersensitive sites in the central nervous system. *Anesthesiology* **86:**760–762.

Franks NP and Lieb WR (1994) Molecular and cellular mechanisms of general anesthesia. *Nature (Lond)* **367:**607–614.

Gallagher MJ and Cohen JB (1999) Identification of amino acids of the *Torpedo* nicotinic acetylcholine receptor contributing to the binding site for the noncompetitive antagonist [^{3}H]tetracaine. *Mol Pharmacol* **56:**300–307.

Galzi J-L and Changeux J-P (1994) Neurotransmitter-gated ion channels as unconventional allosteric proteins. *Curr Opin Struct Biol* **4:**554–565.

Katz EJ, Cortes VI, Eldefrawi ME and Eldefrawi AT (1997) Chlorpyrifos, parathion, and their oxons bind to and desensitize a nicotinic acetylcholine receptor: relevance to their toxicities. *Toxicol Appl Pharmacol* **146:**227–236.

Krasowski MD and Harrison NL (1999) General anesthetic actions on ligand-gated ion channels. *Cell Mol Life Sci* **55:**1278–1303.

Middleton RE, Strnad NP and Cohen JB (1999) Photoaffinity labeling the *Torpedo* nicotinic acetylcholine receptor with [^{3}H]tetracaine, a nondesensitizing noncompetitive antagonist. *Mol Pharmacol* **56:**290–299.

Pedersen SE, Dreyer EB and Cohen JB (1986) Location of ligand binding sites on the nicotinic acetylcholine receptor α subunit. *J Biol Chem* **261:**13735–13743.

Roth SH, Forman SA, Braswell LM and Miller KW (1989) Actions of pentobarbital enantiomers on nicotinic cholinergic receptors. *Mol Pharmacol* **36:**874–880.

Serafini R, Bracamontes J and Steinbach JH (2000) Structural domains of the human $GABA_A$ receptor β3 subunit involved in the actions of pentobarbital. *J Physiol (Lond)* **524:**3649–676.

Smit PH and Kanters JA (1974) The crystal and molecular structure of 5-ethyl-5-(1,3-dimethylbutyl)barbituric acid (α-methylamobarbital). *Acta Crystallogr* **B30:** 784–790.

Scatchard G (1949) The attractions of proteins for small molecules and ions. *Ann N Y Acad Sci* **51:**660–672.

Schild HO (1949) p*Ax* and competitive drug antagonism. *Br J Pharmacol* **4:**277–280.

Smith GR and Sansom MSP (1998) Molecular dynamics study of water and Na^+ ions in models of the pore region of the nicotinic acetylcholine receptor. *Biophys J* **73:**1364–1381.

Tomlin SL, Jenkins A, Lieb WR and Franks NP (1999) Preparation of barbiturate optical isomers and their effects on $GABA_A$ receptors. *Anesthesiology* **90:**1714–1722.

Tonner PH and Miller KW (1995) Molecular sites of general anesthetic action on acetylcholine receptors. *Eur J Anaesthesiol* **12:**21–30.

Unwin N (2000) The Croonian Lecture 2000. Nicotinic acetylcholine receptor and the structural basis of fast synaptic transmission. *Philos Trans R Soc Lond B Biol Sci* **355:**1813–1829.

White BH, Howard S, Cohen SG and Cohen JB (1991) The hydrophobic photoreagent 3- (trifluoromethyl)-3-*m*-([^{125}I]iodophenyl)diazirine is a novel noncompetitive antagonist of the nicotinic acetylcholine receptor. *J Biol Chem* **266:**21595–21607.

White BH and Cohen JB (1992) Agonist-induced changes in the structure of the acetylcholine receptor M2 regions revealed by photoincorporation of an uncharged nicotinic noncompetitive antagonist. *J Biol Chem* **267:**15770–15783.

Yamakura T, Borghese C and Harris RA (2000) A transmembrane site determines sensitivity of neuronal nicotinic acetylcholine receptors to general anesthetics. *J Biol Chem* **275:**40879–40886.

Yost CS and Dodson BA (1993) Inhibition of the nicotinic acetylcholine receptor by barbiturates and by procaine: Do they act at different sites? *Cell Mol Neurobiol* **13:**159–172.

Address correspondence to: Dr. Hugo R. Arias. Department of Pharmacology, School of Medicine, Texas Tech University Health Sciences Center. 3601 4th Street, Lubbock, TX 79430. E-mail: phrhra@ttuhsc.edu